Published in final edited form as:
Int J Remote Sens. 2008 June ; 29(12): 3383–3405. doi:10.1080/01431160701474545.

Remote sensing of ambient particles in Delhi and its environs: estimation and validation

N. KUMAR[*,†], **A. CHU**[‡], and **A. FOSTER**[§]

[†]Department of Geography, 316 Jessup Hall, University of Iowa, Iowa City, IA 52242, USA

[‡]NASA Goddard Space Flight Center, Greenbelt, MD 20771, USA

[§]Department of Economics, Brown University, Providence, RI 02912, USA

Abstract

Recent advances in atmospheric remote sensing offer a unique opportunity to compute indirect estimates of air quality, particularly for developing countries that lack adequate spatial–temporal coverage of air pollution monitoring. The present research establishes an empirical relationship between satellite-based aerosol optical depth (AOD) and ambient particulate matter (PM) in Delhi and its environs. The PM data come from two different sources. Firstly, a field campaign was conducted to monitor airborne particles ≤ 2.5 μm and ≤10 μm in aerodynamic diameter ($PM_{2.5}$ and PM_{10} respectively) at 113 spatially dispersed sites from July to December 2003 using photometric samplers. Secondly, data on eight hourly PM_{10} and total suspended particulate (TSP) matter, collected using gravimetric samplers, from 2000 to 2005 were acquired from the Central Pollution Control Board (CPCB). The aerosol optical depths were estimated from MODIS data, acquired from NASA's Goddard Space Flight Center Earth Sciences Distributed Active Archive Center from 2000 to 2005. Both the PM and AOD data were collocated by time and space: PM mass ± 150 min of AOD time, and ± 2.5 and 5 km radius (separately) of the centroid of the AOD pixel for the 5 and 10 km AOD, respectively. The analysis here shows that PM correlates positively with the 5 km AOD; a 1% change in the AOD explains 0.52% ± 0.20% and 0.39% ± 0.15% changes in $PM_{2.5}$ within 45 and 150 min intervals (of AOD data) respectively. At a coarser spatial resolution, however, the relationship between AOD and PM is relatively weak. But, the relationship turns significantly stronger when monthly estimates are analysed over a span of six years (2000 to 2005), especially for the winter months, which have relatively stable meteorological conditions.

1. Introduction

There has been increasing interest in air quality surveillance and management in the megacities of developing countries for two reasons. Firstly, rising air pollution levels and significant deterioration in air quality are raising public health concerns. Secondly, some megacities, such as Delhi (India) and Lahore (Pakistan), have instituted air quality regulations in recent years. The limited spatial–temporal coverage of air pollution monitoring restricts the ability to study the effect of these regulations on the time–space dynamics of air pollution and, in turn, its effect on human health. Nonetheless, atmospheric remote sensing and chemical transportation models can be exploited to assess indirect estimates of air pollution. Both methods have been successfully employed and tested to assess indirect estimates of fine particles ≤ 2.5 μm in aerodynamic diameter ($PM_{2.5}$) and

[*]Corresponding author. naresh-kumar@uiowa.edu.

coarse particles ≤ 10 μm (PM_{10}), and aerosol type and loading (e.g. Carmichael et al. 2003, Wang and Christopher 2003, Tang *et al*. 2004, Chu *et al*. 2005, Petrakis *et al*. 2005, Gupta *et al*. 2006), but at a coarse spatial resolution (>10 km). The chemical transportation model requires emission inventory data that are scarcely available or up-to-date, especially for developing countries. Therefore, atmospheric remote sensing is the only solution to compute indirect estimates of air quality at high spatial–temporal resolutions in the absence of air pollution data.

Satellite sensors record electromagnetic radiation from the earth's surface, and when the radiation traverses through the atmosphere it interacts with aerosols (fine solid and/or liquid particles suspended in the air) prior to reaching the sensors that are mounted onto satellites. The distortion in the beam power through this interaction is used to estimate aerosol loading, which is also known as aerosol optical depth/thickness (AOD). Recent literature suggests that the ground measurements of $PM_{2.5}$ and PM_{10} correlate positively with the AOD at a coarser spatial resolution ≥ 10 km (e.g. Sifakis *et al*. 1998, Chu *et al*. 2002, Chu *et al*. 2005, Petrakis *et al*. 2005, Gupta *et al*. 2006, Kumar *et al*. 2007). Although data from various satellites can be used to compute the AOD, data from Moderate Resolution Imaging Spectroradiometers (MODIS) onboard the Terra and Aqua satellites are particularly useful, because these satellites have a daily repetitive global coverage, meaning that daily air quality surface, which is required to assess short-term exposure to air pollution, can be estimated.

Using the data from the MODIS onboard the Terra Satellite, this paper examines the association of AOD (at 5 and 10 km spatial resolutions) with $PM_{2.5}$ and PM_{10} data observed on the ground at two geographic scales and using two different sources of PM data. This will aid in the understanding of the effectiveness of satellite-based AOD data in predicting indirect estimates of airborne fine and coarse particles, which have been widely accepted as the standard measures of air quality (WHO 2000, 2006). Although the existing literature supports a positive association between airborne particles and AOD, the intensity of this association varies regionally (Wang and Christopher 2003, Chu *et al*. 2005, Gupta *et al*. 2006), because the sources and composition of aerosols and meteorological conditions also vary regionally. Therefore, it is important to validate this association regionally prior to predicting $PM_{2.5}$ and PM_{10} values with the aid of AOD data.

The need for this work emerged from the desire to model the effects of improvement in air quality on respiratory health in Delhi, which is the only megacity in northern India (figure 1), and which has instituted a series of air quality regulations in recent years. The areas surrounding Delhi, however, are largely unaffected by these regulations. Due to the non-availability of spatially detailed air pollution data, the potential of satellite remote sensing to assess indirect estimates of air pollution was explore, and this paper is the result of the explorations. The potential of satellite remote sensing to predict air quality by establishing an empirical relationship of AOD (from MODIS data at two different spatial resolutions of 5 and 10 km) with the ambient particles observed on the ground after accounting for the effect of meteorological conditions is demonstrated. This relationship will form the base to predict surface levels of ambient particles before and after the air quality regulations, which will allow the effect of the regulations on the time–space dynamics of air pollution, and its effect, in turn, on human health to be assessed.

2. Data and methods

2.1 Data

The data for this research has been obtained from five different sources: (a) ambient particles monitored at 113 sites in Delhi and its environs, (b) PM_{10} data from the Central

Pollution Control Board, Delhi, India, (c) Terra MODIS, (d) the Indian Meteorological Department, and (e) the National Climatic Data Center.

2.1.1 Air pollution monitoring field campaign—A field campaign was conducted from 23 July to 3 December 2003 to monitor PM at 113 sites in Delhi and its surroundings. Since one of the major goals of the campaign was to evaluate spatial variability in the mass of $PM_{2.5}$ and PM_{10}, a spatially dispersed sampling design was adopted, in which sample sites were identified using a two-step process. In the first, a rectangular grid was overlaid onto the entire study area, to ensure full coverage of the area. In the second step, a random location was simulated within each cell (of size 1 × 1.5 km), and then the simulated locations were transferred to a Garmin Global Positioning System (GPS) in order to navigate them and examine their suitability. Some sites, which were inaccessible, were discarded and re-simulated, resulting in a final sample of 113 suitable sites that are shown in figure 2. Further details on the sampling method are available in Kumar and Foster (2007). At each site, air was sampled at two different times every third day. Each sample involved four readings, two in mass mode and two in count mode. Each reading sampled air for 2 min in the mass mode, and for 1 min in the count mode. Therefore, each sample involved 6 min of sampling. Although air was sampled at different times between 7:30 a.m. and 10:00 p.m., the PM data for the present analysis was restricted to ± 150 min of the time interval of AOD data (generally 10:30 a.m.) in order to minimize temporal noise in the PM Data.

The Aerocet 531, a photometric sampler, from Met One Instruments Inc. (2003), was used to collect air pollution data. It is an automatic instrument that can monitor the PM mass of particles ≤ 1, ≤ 2.5, ≤ 7 and ≤ 10 μm in aerodynamic diameter, and number of particles ≤ 0.5 and PM ≤ 10 μm. The instrument uses laser technology and uses a right angle scattering method at 0.78 μm, which is different from gravimetric measurements. The source light travels at a right angle to the collection system and detector, and the instrument uses the information from the scattered particles to calculate a mass per unit volume. A mean particle diameter is calculated for each of five different sizes. This mean particle diameter is used to calculate a volume (m^3), which is then multiplied by the number of particles and then a generic density ($\mu g\ m^{-3}$) that is a conglomeration of typical aerosols. The resulting mass is divided by the volume of air sampled for a mass per unit volume measurement ($\mu g\ m^{-3}$).

2.1.2 PM Data from the Central Pollution Control Board (CPCB)—One of the 113 sites was located parallel to the air pollution monitoring station near the Income Tax Office (ITO). This station is operated by the CPCB and monitors ambient air pollution and collects data on various pollutants including PM_{10} and TSP matter. Data were acquired from the CPCB from the year 2000 through to 2005. PM_{10} data were collected in three different shifts 6:00 to 14:00, 14:00 to 22:00 and 22:00 to 6:00 (of the next day) using high-volume samplers. This station, however, was not equipped to monitor $PM_{2.5}$. While the data from the field campaign site near the ITO enabled the differences in PM_{10} values to be compared across photometric and gravimetric (conventional) samplers, the CPCB data from 2000 and 2005 enabled the robustness of the association between AOD and PM_{10} to be assessed.

2.1.3 Satellite data—Data from the MODIS onboard the Terra satellite was used because one of the long-term goals of the research here is to longitudinally study the effect of air quality regulations on the time–space dynamics of air pollution in Delhi from 2000 to 2005. The Aqua satellite, however, was launched in the year 2002, and hence data from Aqua are not available prior to the year 2002 (i.e. before the adoption of air quality regulations). Data from MODIS (onboard Terra) were acquired from NASA's Goddard Earth Sciences Distributed Active Archive Center (DAAC). Although air pollution data were recorded from July to December, satellite data were acquired for the months of October and November 2003 because of stable meteorological conditions during these two months. During this two

month period, the AOD data was extracted for all cloud-free days at a 5 km spatial resolution. The 10 km AOD data from 2000 to 2006 were extracted from the AOD products acquired from the DAAC at NASA.

2.1.4 Meteorological data—A probe was used with the Aerocet 531 instrument to record temperature and relative humidity of each sample. Other meteorological data, such as atmospheric pressure, wind velocity, wind direction and rainfall were acquired from the Indian Meteorological Department at 3 h intervals, and daily meteorological data were acquired from the National Climatic Data Center from 2000 to 2005.

2.2 Methods

2.2.1 Data pre-processing—The data pre-processing involved two important steps. In the first, the field campaign data were extracted for the months of October to November 2003, as these two months experienced relatively stable meteorological conditions in the study area. Since each sample recorded two readings in the mass mode, the average of these two readings was computed for estimating the mass of the $PM_{2.5}$ and PM_{10} values.

The spatial and temporal resolutions of AOD and PM data were different. Therefore, in the second step, PM data (from the field campaign and the CPCB) were collocated with the satellite-based AOD data at different spatial–temporal resolutions. As mentioned earlier, air pollution data from the field campaign were collected at 113 sites, and AOD values from the MODIS data were at 5 and 10 km pixel resolutions (at nadir), which created the problem of geographic misalignment. For example, on a given day, two or more sample sites could be located in a 5 km AOD pixel, and this number could be significantly higher for the 10 km AOD. Therefore, data were integrated using both a one-to-many (one AOD value for all points within in a pixel) as shown in figure 3 and a many-to-one (average value of PM at many sample sites in one AOD pixel) relationship. This resulted in two different datasets and enabled $PM_{2.5}$ and PM_{10} to be modelled as a function of AOD at the spatial resolution of the sampling locations (a disaggregated level without losing any geographic details) and at the AOD pixel level, in which PM data (collected at a point location) were aggregated to match the spatial resolution of the AOD data.

Although the CPCB monitors air pollution at several sites, only one site mentioned above has been in continuous operation for the past several years. This provided an opportunity to examine the trend of the association between AOD and PM_{10} from 2000 to 2005. The 10 km AOD and PM_{10} data were matched by the date and different distances from the CPCB site at the ITO to the centroid of each AOD pixel. This enabled the association of PM_{10} with the AOD aggregated at different distance intervals to be examined.

2.2.2 Aerosol estimation—Aerosols are solid and liquid particles suspended in the air, and AOD can be defined as the extinction in the beam power due to the presence of aerosols in the atmosphere. The AOD typically decreases with increasing wavelength for fine-mode dominated aerosols. Visible spectral bands of various remote sensing satellites have been exploited to estimate AOD over both water and land surfaces (e.g. Holben *et al*. 1992, Sifakis *et al*. 1998, King *et al*. 1999, Christopher *et al*. 2000, Chu *et al*. 2003, Wang and Christopher 2003, Chu *et al*. 2005, Petrakis *et al*. 2005). In essence, AOD (τ) at a given site (s) is the log of the ratio of irradiance at the top of the atmosphere (I_o) to irradiance at the same location at the surface (I_s) (Hapke 1993). Scattering due to the presence of aerosol increases and decreases the beam power towards and away from the direction of the sensor Ω respectively. The effect of aerosol loading (due to scattering and/or absorption) on radiance recorded by the sensor can be computed using a radiative transfer model (Kaufman *et al*. 1997, King *et al*. 1999).

Aerosol retrieval over land is further complicated by the fact that the land surface shows a large variability in reflection, from dark vegetation to bright desert and snow/ice-covered regions. Due to the competing processes of surface reflection and aerosol backscattering in radiative transfer, radiance measured with less surface interference results in a smaller uncertainty in the retrieved aerosol properties. The dark target approach is based on the correlation between the chlorophyll absorption of vegetation in the visible spectrum (0.47 and 0.66 μm) and liquid water absorption at 2.1 μm (reflectance<0.25). The fine-mode particles (urban/industrial and biomass-burning aerosols) are transparent at 2.1 μm (i.e. minimal aerosol effect), which allows direct observation of the earth's surface (even through heavy pollution) to estimate the surface reflectance in the visible spectrum. The MODIS AOD is computed at 0.47 and 0.66 μm by matching the averaged reflectance (after screening for clouds, water and snow/ice pixels from a total of 100 pixels) on a 5×5 km^2 grid to the value of a pre-calculated lookup table under the same Sun–satellite geometrical condition. The selection of 5×5 km^2 is mainly due to a large surface variability on a global scale. It can be enhanced to meet different requirements of applications (e.g. urban air quality) under proper conditions. In general, the errors are $\pm 0.05\tau_a$ and $\pm 0.20\tau_a$ over vegetated and semi-vegetated regions, respectively (Chu *et al*. 2002).

The lookup table is constructed using Dave's code (Dave and Gazdag 1970), which assumes a spherical particle shape, an 'average' aerosol profile, and lognormal size distributions (Chu *et al*. 2003). Three general aerosol types have been considered: urban/industrial pollution, biomass-burning aerosols, and dust. The spectral aerosol path adiance is used to separate dust from the other two types, because dust particles are significantly larger than pollution or smoke particles. Mixture of dust and non-dust aerosols is taken into account by the fine-mode fraction obtained from the linear interpolation from the derived path radiance ratio and the assumed ratio of dust and pollution (or smoke) models. Since pollution and biomass-burning aerosols are both dominated by fine-mode particles, they are distinguished by *a priori* assumptions based on geography varying with season. Using this methodology, AOD values were computed for 40 days to match with the field campaign PM data. The 10 km AOD data were extracted from the Terra Atmospheric Products, and the details on the 10 km AOD computation are available in Remer *et al*. (2006).

2.2.3 Statistical modelling—The AOD values were computed using MODIS data at 5 km spatial resolution, and 10 km AOD values were acquired from NASA's Goddard Space Flight Center Earth Sciences Distributed Active Archive Center. Since the spatial resolutions of PM and AOD data were different, it posed the problem of geographic misalignment. Therefore, the analyses were pursued on two different geographic scales: at point level and at AOD pixel level. At the point level, a one-to-many relationship was used to integrate AOD data with the PM data, and the same AOD was assigned to all points within the pixel; this will be referred to as '*disaggregated*' data from now on. At the pixel level, however, PM data were integrated using a one-to-one relationship, in which PM data were aggregated (by averaging PM of all points within an AOD pixel) to match the spatial resolution of the AOD data, which will be referred to as '*aggregated*' from now on. Since the data are on two different geographic scales, two different sets of regression models were required. In the aggregated analysis, a simple regression method was used to model average PM (either $PM_{2.5}$ or PM_{10}) for the *j*th pixel as a function of AOD at the *j*th pixel and meteorological conditions:

$$\mathrm{PM}_j = \alpha + \beta\tau_j + \lambda \mathbf{w}'_j + \left(\sigma^2_{\mathrm{PM}_{ij}} + \varepsilon_j\right), \quad (1)$$

where PM_j is the average PM (either $PM_{2.5}$ or PM_{10}) for the *j*th pixel, τ_j is the AOD value estimated from MODIS data at the *j*th location, $\mathbf{w}'_j$ is a matrix of confounders, including relative humidity and temperature, σ^2_{PMij} is the intra-pixel variance in PM, also referred to as intra pixel noise, and ε_j is the error term.

The regression model in equation (1) was also employed to validate the association between AOD and PM_{10} data collected from the CPCB for 2000 to 2005. Since there was only one site that monitored PM_{10} for the entire duration, the average monthly AOD was computed within different distance radii from the ITO site. In the final analysis, however, monthly estimates of AOD within 0.1° were included, for these showed the best association between monthly AOD and PM_{10}.

In the disaggregated analysis, the PM at the *i*th sample site located in the *j*th pixel was modelled as a function of AOD (τ) of the pixel and meteorological conditions (as in equation (2)). All sample sites (in a given day) within a pixel were assigned the same AOD value. This resulted in an intra-pixel correlation structure in AOD. Therefore, to control this correlation structure, a pixel-level random effect δ_j was introduced to compute pixel-level independent estimates:

$$PM_{2.5ij}=\alpha+\beta\tau_j+\lambda\mathbf{w}_{ij}+\left(\delta_j+\varepsilon_{ij}\right), \tag{2}$$

where δ_j is the 5 km pixel-level random effect.

Direct evaluation of the predictive power of the model is complicated by the fact that the PM measurements are effectively sampled at a different resolution to the AOD measurements. In particular, it would be desirable to know the predictive value of the AOD in terms of the average true PM at the level of an AOD pixel. The problem is that only a small sample of the PM measurements at the pixel level exists, and thus the R^2 from equation (2) will underestimate the percentage of variation that could be explained for the average PM measurements (averaged across all possible sites in a given AOD pixel). However, this estimate can be constructed from the estimated random-effects errors:

$$R^2_{\text{pixel}}=1-\text{Var}(\delta_j)/[\text{Var}(PM_{2.5ij})-\text{Var}(\varepsilon_{ij})]. \tag{3}$$

3. Results

3.1 Data validation – photometric and gravimetric measurements

Since spatially detailed PM data were not available for the study area, a field campaign to collect these data using photometric samplers was conducted. Conventionally, high volume samplers are employed to monitor ambient PM, which requires a minimum of 8 h of sampling. Filters are weighed before and after the sampling, and based on the mass gained during the sampling period and the amount of air sampled, the mass of PM is computed. The AOD estimates from the satellite, however, represent a very limited time window of less than 1 min, as sensors (mounted onto satellites) record the electromagnetic field when crossing a location. The overpass time of the Terra satellite is 10:30 a.m. Therefore, photometric samplers were employed to monitor PM in real time so that PM data (monitored) on the ground could be matched with the AOD time (10:30 a.m.) as closely as possible; PM data were restricted to ±150 min of AOD time, as beyond this interval, the association between PM and AOD begins to drop significantly.

During August through to November 2003, the daily averages of PM_{10} from the CPCB site and our instrument were 203 ± 26.8 μg m^{-3} and 153 ± 33.5 μg $m^{-}{}_{3}$ respectively. As reported in other studies (Ramachandran *et al*. 2003), the photometric estimates were significantly lower than the gravimetric estimates. Given the differences in the method of operation and duration of sampling by gravimetric (24 h average) and real time photometric measurements (4 min for each sample), a difference of 49.5 ± 31 μ gm^{-3} at the 95% confidence interval (CI) seems reasonable. In addition, the regression analysis shown in figure 4 suggests a statistically significant positive association in the temporal variability in PM_{10} measured by both methods. It was not possible to validate $PM_{2.5}$ because of the non-availability of $PM_{2.5}$ data from any sources in the study area. Based on other research, the difference between photometric and gravimetric estimates is likely to be smaller for $PM_{2.5}$. Although the photometric estimates can be calibrated to gravimetric standards by adjustment for relative humidity, as suggested by Ramachandran *et al*. (2003), these data were not calibrated in the present study. This is because the calibration will be constant for all sites in a given day and the main goal here was to assess the effectiveness of the AOD in predicting the spatial–temporal variability in the PM, rather than the absolute estimates of the PM.

3.2 Spatially detailed PM and AOD data, October–November 2003

The aggregate estimates of AOD from October through to November 2003 were analysed at 5 and 10 km spatial resolutions. These data were aggregated and interpolated values of 5 and 10 km AOD were estimated at the 113 sampling sites. Descriptive statistics of $PM_{2.5}$, PM_{10} and AOD data at both spatial resolutions is presented in table 1. In the table, aggregate AOD estimates were assigned to the 113 monitoring sites. While the concentration of PM varies greatly inside Delhi, the AOD concentration varies significantly outside Delhi, although the AOD variance is much lower than the variance in the PM. The average concentrations of $PM_{2.5}$ and PM_{10} between August and November 2003 in Delhi were recorded as 82.9 ± 7.8 μg m^{-3} (at 95% CI) and 304.2 ± 29.8 μg m^{-3} (at 95% CI) respectively, which are significantly higher than the standards recommended by the Environmental Protection Agency (EPA 2006) and the World Health Organization (WHO 2006). This leads to the conclusion that the state of air quality in Delhi is poor even with the enforcement of compressed natural gas (CNG) and other regulations.

The average AOD measurements inside Delhi were reported as 0.64 ± 0.023 and 0.65 ± 0.025 at 5 and 10 km spatial resolutions respectively. The average AOD values were also computed with reference to the distance from the city centre (Connaught Place). Table 2 shows a gradual decline in the average AOD with increasing distance from the city centre; the AOD concentration drops from 0.664 within 0.1° (about 9.17 km) of the city centre to 0.545 within 0.5° (about 48.5 km). The gradient of decline in the AOD is higher at 5 km spatial resolution than at 10 km.

In the preliminary analysis, $PM_{2.5}$ and PM_{10} were regressed on 5 and 10 km AODs. Given the substantial variability in $PM_{2.5}$ and PM_{10} within 10 km pixels, $PM_{2.5}$ and PM_{10} did not show a strong relationship with AOD. Although both $PM_{2.5}$ and PM_{10} observed significant variability within 5 km pixels, AOD at this spatial resolution emerged as an important predictor of both $PM_{2.5}$ and PM_{10}. The results of disaggregated and aggregated analyses are presented in tables 3 and 4 respectively. The analysis was conducted separately at 15 min intervals within ± 150 min of the overpass time of the Terra satellite (generally 10:30 a.m. local time). In the tables, robust *t* statistics are in parentheses, * indicates values that are significant at 5% and ** indicates those that are significant at 1%.

Since local meteorological conditions can greatly influence aerosol loading, the effect of different meteorological conditions, such as wind velocity, relative humidity, temperature and atmospheric pressure, was examined along with AOD. Among these, relative humidity

and atmospheric pressure, which also witnessed significant association with wind direction, were used in the final analysis. Both relative humidity and sea level atmospheric pressure showed a statistically significant impact on both $PM_{2.5}$ and PM_{10}. While relative humidity can distort the PM mass by inflating the particle size, atmospheric pressure is linked to mobility in the particles, for example low pressure may result in high mobility in fine particles. From both disaggregated and aggregated analyses, it is evident that $PM_{2.5}$ is more sensitive to relative humidity and atmospheric pressure than PM_{10}.

The 5 km AOD data show a statistically significant positive association with $PM_{2.5}$ and PM_{10} (see tables 3 and 4). At the disaggregate level, a 1% change in AOD explains a 0.398%±0.151% (95% CI) change in $PM_{2.5}$ and 0.207%±157% (95% CI) change in PM_{10} within ±150 min of the AOD data. The predictive power of AOD is much stronger for shorter time intervals. For example, within a 45 min time interval, a 1% change in AOD (holding other variables constant) explains 0.52% and 0.45% changes in $PM_{2.5}$ in the disaggregate and aggregate analyses respectively. In the study area, the concentration of both types of PM varies significantly. Consequently, the daily estimate of PM for a given pixel can be noisy. But after this noise into account, as in equation (3), the R^2 value increases substantially; within a ± 15 min interval, the R^2 values increased to 76% and 81% for $PM_{2.5}$ in the disaggregate and aggregate analyses respectively (tables 3(*a*) and 4(*a*)).

3.3 PM_{10} and AOD data from 2000 to 2005

As mentioned earlier, PM_{10} data are available for one site in the study area for the past several years, and MODIS AOD products from NASA are available from 2000 onward (from the Terra Satellite). The 10 km AOD data were extracted around this site and matched with the PM_{10} data by date. The daily PM_{10} value at the ITO site does show a stronger association with the daily AOD (figure 5(*a*)) as compared to monthly estimates of AOD and PM_{10} values (figure 5(*b*)). There can be several reasons for this. Firstly, PM_{10} data were 8 and 24 h estimates, while AOD data were calculated using the MODIS satellite data that covers the study area around 10:30 a.m. every day. Thus, there were substantial mismatches in the temporal resolution of these two datasets. Secondly, enormous variation was observed in PM_{10} and AOD data during the two months before and after *monsoon* season because of many dust storms in the pre- and post-monsoon periods. During the monsoon seasons, however, most particles, particularly the coarse ones, are flushed away due to rain, and it takes several days before the normal range of PM is attained. Figure 5(*a*) clearly shows the instability in PM_{10} and AOD estimates during the monsoon and pre-monsoon seasons. Therefore, the final analysis was restricted to winter months only, and outliers were removed from the analysis. To account for extreme values, AOD values greater than 1.5 were excluded; these accounted for less than 5% of the observations.

Descriptive statistics of AOD, PM_{10} and total suspended particles (TSP) are shown in table 5. The monthly average of AOD during 2000 to 2002 was 0.80 ± 0.024 (95% CI), which declined to 0.71 ± 0.018. The decline in AOD was statistically significant and, likewise, a decline was also observed in SO_2 and TSP. Two other pollutants, namely NO_2 and PM_{10}, however, registered statistically significant increases in the post-regulation periods, which is contradictory to the decline reported in other pollutants. Therefore, readers should take care interpreting the results in table 5, because the AOD statistics presented in this table did not account for the influence of meteorological conditions and data on other pollutants monitored, as one site alone cannot represent the state of air quality for the entire city. In addition, contradictory trends of PM_{10} and TSP in pre- and post-regulation periods question the reliability of the instruments used in monitoring these data.

Regression analysis shows a statistically significant positive association of monthly AOD values with the monthly averages of PM_{10} and TSP values (figure 5(*b*) and table 6). The

association between AOD and both PM_{10} and TSP is strongest in the morning shift (6:00–14:00), which is obvious given that the AOD data represent air quality at around 10:30 a.m. (figure 5(*b*)). One unit increase in the log of AOD explains 177 and 300 $\mu g\ m^{-3}$ increases in PM_{10} and TSP values respectively, keeping relative humidity and atmospheric pressure constant. AOD values, in association with relative humidity and atmospheric pressure, explain 53% and 45% of the total variability in the PM_{10} and TSP respectively. The difference in the temporal resolution of the AOD and PM data could be one of key explanations for the low R^2 values.

3.4 Spatial patterns of AOD, $PM_{2.5}$ and PM_{10} data

Figures 6 and 7 show average estimates of AOD during October and November 2003, and figures 8 and 9 show interpolated surfaces of $PM_{2.5}$ and PM_{10} values from August to November 2003. While there are many similarities in the spatial distribution of the PM and AOD data, the spatial variation in the PM does not perfectly coincide with the variation in AOD. There are two main explanations for this. Firstly, the AOD estimates span across only two months, October to November, while the PM estimates cover the period from August to November. Secondly, the geographic scale of these two datasets is different, AOD are 5 and 10 km pixels (area) data, and PM are interpolated using point data.

Manufacturing units and transport are two major sources of emission in the Delhi. An interesting finding that has emerged from these maps is that the areas in and around industrial clusters observe elevated concentrations of both PM and AOD, except in the south-western part of the study area. While CNG regulations (implemented from 2000 to 2002) are expected to have a major impact on the concentration of fine particles ($PM_{2.5}$), unabated increase in personal vehicles (such as cars, scooters and motorcycles) continue to be an important sources of ambient particles (Kumar and Foster 2007). The average concentrations of both 5 and 10 km AOD data gradually decline with the increasing distance from the city centre. The average concentration of AOD (τ) in the north-eastern parts of Delhi was more than 0.6, and the values outside Delhi boundaries are less than 0.5.

4. Discussion

This article evaluated the association between PM and AOD data using aggregated and disaggregated data. As far as the trend of the association between the 5 km AOD and PM concentration is concerned, the results here are consistent with the findings of previous literature (Chu *et al*. 2003, Gupta *et al*. 2006). In the spatially detailed analysis, the AOD, in association with relative humidity and sea level atmospheric pressure, explains more than 70% variability in $PM_{2.5}$ and PM_{10} within ± 150 min of the overpass window of the ESO Terra satellite; these estimates account for intra-pixel noise in PM. The PM–AOD association in Delhi, however, is weaker than that reported in other parts of the world (Chu *et al*. 2005, Gupta *et al*. 2006). The monthly AOD–PM association at the ITO site from 2000 to 2005 was statistically significant and stronger, and could predict about 50% of the total variability in PM_{10} and TSP. As described above, the concentration of PM varies significantly across space and time. Thus, it is critically important to match the spatial–temporal resolutions of AOD and PM data as closely as possible.

The standard AOD products from NASA are available at 10 km spatial resolution. The main goal here was to predict $PM_{2.5}$ and PM_{10} data at a high spatial resolution to compute human exposure to ambient particles. Therefore, AOD estimates at 5 km spatial resolution were computed and compared to the standard 10 km AOD products. The analysis here suggests that daily estimates of AOD at 10 km spatial resolution cannot effectively predict spatially detailed daily air pollution surfaces. Nevertheless, when these data were aggregated, the standard 10 km AOD products can be useful to predict monthly estimates of PM_{10} and TSP,

but the predictive power of AOD is relatively low, because the MODIS AOD products are likely to influenced by an excessive concentration of dust during the pre-monsoon season (Tripathi *et al*. 2005), and precipitation during the actual monsoon can flush away ambient particles, frequently resulting in too much noise in both the PM and AOD data. Therefore, the data for pre-monsoon and monsoon seasons should be avoided in order to construct a long-term time-series profile of ambient particles for the megacities, which lack reliable air pollution data.

There is a growing interest in the use of spatially detailed AOD data for air quality surveillance and health effect research (Kumar *et al*. 2007), and researchers are attempting to estimate AOD data at a high spatial resolution (Li *et al*. 2005, Kumar *et al*. 2007). The field campaign data collected here at 113 sites show significant spatial–temporal variability in PM values. Moreover, the predictive power of 10 km AOD is weaker than that of the 5 km AOD. Our future research will be geared towards improving algorithms for computing AOD at 2.5 and 1 km spatial resolutions and their association with the spatially detailed PM data.

The mismatch between the temporal resolution of PM and AOD data is another important challenge, as AOD estimates are computed from sensors onboard different satellites (which record the electromagnetic field within a very limited time window of less than 1 min), and the available PM data are generally collected using high volume samplers, which sample air for at least 8 h. The extremely short time window of AOD data is thus significantly smaller than the 8 h duration of sampling for PM data. The use of photometric samplers, as demonstrated in this article, is one potential solution. These samplers can record PM in real time. Our analysis reveals that $PM_{2.5}$ and PM_{10} observe the best association with AOD ±45 min and ± 75 min time windows of AOD data respectively. These findings have important implications for research that aims to study the relationship between AOD and PM in different parts of the world and for air quality monitoring strategies.

In the absence of air pollution data at high spatial–temporal resolutions, researchers have begun to explore the potential of AOD to predict air quality in megacities in developing countries. Given the regional variations in the nature and sources of aerosols, the association between PM and AOD values can vary regionally (Gupta *et al*. 2006). This will require a field experiment to collect real-time air pollution data using passive samplers, as demonstrated by Kumar *et al*. (2007). This is because existing air pollution monitoring relies on the gravimetric method, which requires samplers to run for eight or more hours, and the PM concentration reported from these samplers is the average for this duration, which can be quite noisy for the PM–AOD association. Nevertheless, using photometric samplers (installed onto mobile labs), spatially detailed data can be collected frequently and inexpensively. Based on the findings of this research, we suggest 9:00 a.m. to 3:00 p.m. as an ideal time window for collecting PM data on the ground, which then allows AOD data from MODIS onboard both Terra (morning) and Aqua (afternoon) satellites to be examined.

A host of factors such as sources of air pollution, proximity to water bodies, vegetation, seasonality and meteorological conditions, all of which vary regionally, can influence aerosol loading and hence its relationship with PM. Therefore, the AOD–PM association observed in one city cannot be extrapolated to others, and will require additional field experiments before AOD can be used to predict air pollution. Future research should also aim to examine the AOD–PM association with reference to sources of air pollution, land-use type and aerosol characterization. This article demonstrated a visual association between sources of air pollution – namely industrial locations and main roads – and the concentration of AOD and PM. Another interesting finding of the research here is the diminishing level of

AOD with the increasing distance from the city centre, which clearly shows that air pollution distribution in the study area is an inverse function of distance from the city centre.

The results reported in this research can be used to predict $PM_{2.5}$ and PM_{10} surfaces since the year 2000 at the 5 km spatial resolution, and monthly estimates of PM_{10} and TSP at 10 km spatial resolution. Although 5 km spatial resolution is inadequate to compute exposure to ambient air pollution, it can certainly be valuable to examine the time–space dynamics of air pollution in response to recently enacted environmental laws in Delhi. The future research to compute $PM_{2.5}$ and PM_{10} surfaces from AOD at high spatial resolution is likely to pave the way to compute exposure to ambient air pollution for health research.

Acknowledgments

We gratefully acknowledge MODIS data from NASA, meteorological data from the National Climatic Data Center and air pollution data from the Central Pollution Control Board, Government of India, Delhi. The funding support for this work come from the Population Studies and Training Center, Brown University and NICHD/NIH (5 R21 HD046571-02). We are also thankful to Mr V. Kumar, Dr O.P. Malik and Mr A. Kumar for coordinating air pollution data collection, to Professor O.P. Sharma, IIT, Delhi, India for the logistic support and to the anonymous referees for their valuable comments.

References

Carmichael GR, Tang Y, Kurata G, Uno I, Streets DG, Thongboonchoo N, Woo J-H, Guttikunda S, White A, Wang T, Blake DR, Atlas E, Fried A, Potter B, Avery MA, Sachse GW, Sandholm ST, Kondo Y, Talbot RW, Bandy A, Thorton D, Clarke AD. Evaluating regional emission estimates using the TRACE-P observations. Journal of Geophysical Research. 2003; 108:8810.

Christopher SA, Chou J, Zhang J, Li X, Welch RM. Shortwave direct radiative forcing of biomass burning aerosols estimated from VIRS and CERES. Geophysical Research Letters. 2000; 27:2197–2200.

CHU, DA. Analysis of the relationship between MODIS aerosol optical depth and PM2.5 over the summertime U.S. In: Chu, A.; Szykman, J.; Kondragunta, S., editors. Remote Sensing of Aerosol and Chemical Gases, Model Simulation/Assimilation and Applications; Proceedings of SPIE; San Diego, CA: SPIE Digital Library; 2006. p. 6299p. 629903-629909.

Chu DA, Kaufman YJ, Ichoku C. Validation of MODIS aerosol optical depth retrieval over land. Geophysical Research Letters. 2002; 29:8007.

Chu DA, Kaufman YJ, Zibordi G, Chern JD, Mao J, Li C, Holben BN. Global monitoring of air pollution over land from EOS-Terra MODIS. Journal of Geophysical Research. 2003; 108:4661.

Dave JV, Gazdag J. A modified Fourier transform method for multiple scattering calculations in a plane parallel Mie atmosphere. Applied Optics. 1970; 9:1457–1466. [PubMed: 20076400]

Environmental Protection Agency (EPA). Revisions to Ambient Air Monitoring Regulations: Proposed Rule (Amendments). Office of Research and Development, Environmental Protection Agency; Research Triangle Park, NC: 2006.

Gupta P, Christopher SA, Wang J, Gehrig R, Lee YC, Kumar N. Satellite remote sensing of particulate matter and air quality assessment over global cities. Atmospheric Environment. 2006; 40:5880–5892.

Hapke, B. Theory of Reflectance and Emittance Spectroscopy. Cambridge: Cambridge University Press; 1993.

Holben BN, Vermote E, Kaufman YJ, Tanré D, Kalb V. Aerosol retrieval over land from AVHRR data – application for atmospheric correction. IEEE Transactions on Geoscience and Remote Sensing. 1992; 30:212–222.

Kaufman YJ, Wald AE, Remer LA, Bo-Cai G, Rong-Rong L, Flynn L. The MODIS 2.1 μm channel correlation with visible reflectance for use in remote sensing of aerosol. IEEE Transactions on Geoscience and Remote Sensing. 1997; 35(5):1286–1298.

King MD, Kaufman YJ, Tanre D, Nakajima T. Remote sensing of tropospheric aerosols from space: past, present and future. Bulletin American Meteorological Society. 1999; 80:2229–2259.

Kumar N, Chu A, Foster A. An empirical relationship between $PM_{2.5}$ and aerosol optical depth in Delhi Metropolitan. Atmospheric Environment. 2007; 41:4492–4503.

Kumar N, Foster A. Air quality interventions and spatial dynamics of air pollution in Delhi and its surroundings. International Journal of Environment and Waste Management. 2007 (in press).

Li C, Lau AK-H, Mao JT, Chu DA. Retrieval, validation and application of 1-km resolution aerosol optical depth from MODIS data over HongKong. Transactions on Geoscience and Remote Sensing. 2005; 43:2650–2658.

Met One Instruments Inc. AEROCET 531: Operation Manual. OR: Grants Pass; 2003.

Petrakis M, Kopiana T, Psiloglou B, Briggs D, Hoek G, Asbjorn A, Shaddick G, Sifakis N, Petalis A. GIS and remote sensing techniques in emission mapping for health management in Europe. IASME Transactions. 2005; 2:383–388.

Ramachandran G, Adgate JL, Pratt GC, Sexton K. Characterizing indoor and outdoor 15 minute average PM2.5 concentrations in urban neighborhoods. Aerosol Science and Technology. 2003; 37:33–45.

Remer, LA.; Tanré, D.; Kaufman, YJ. Algorithm for remote sensing of tropospheric Aerosol from MODIS. Goddard Space Flight Center, NASA; 2006.

Sifakis N, Soulakellis N, Paronis D. Quantitative mapping of air pollution density using Earth observations: a new processing method and application on an urban area. International Journal of Remote Sensing. 1998; 19:3289–3300.

Tang Y, Carmichael GR, Kurata G, Uno I, Weber RJ, Song C-H, Guttikunda SK, Woo J-H, Streets DG, Wei C, Clarke AD, Huebert B, Anderson TL. Impacts of dust on regional tropospheric chemistry during the ACE-Asia experiment: a model study with observations. Journal of Geophysical Research (Atmospheres). 2004; 109(D19S21)

Tripathi SN, Dey S, Chandel A, Srivastava S, Singh RP, Holben BN. Comparison of MODIS and AERONET derived aerosol optical depth over the Ganga Basin, India. Annales Geophysicae. 2005; 23(4):1093–1101.

Wang J, Christopher SA. Intercomparison between satellite-derived aerosol optical thickness and PM2.5 mass: implications for air quality studies. Geophysical Research Letters. 2003; 30:2095-1–4.

World Health Organization (WHO). Guidelines for Air Quality. Geneva: World Health Organization; 2000.

World Health Organization (WHO). WHO Air Quality Guidelines for Particulate Matter, Ozone, Nitrogen Dioxide and Sulfur Dioxide – Global update 2005 – Summary of Risk Assessment. Geneva: World Health Organization; 2006.

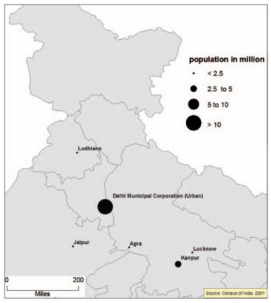

Figure 1.
Major cities in northern India, 2001.

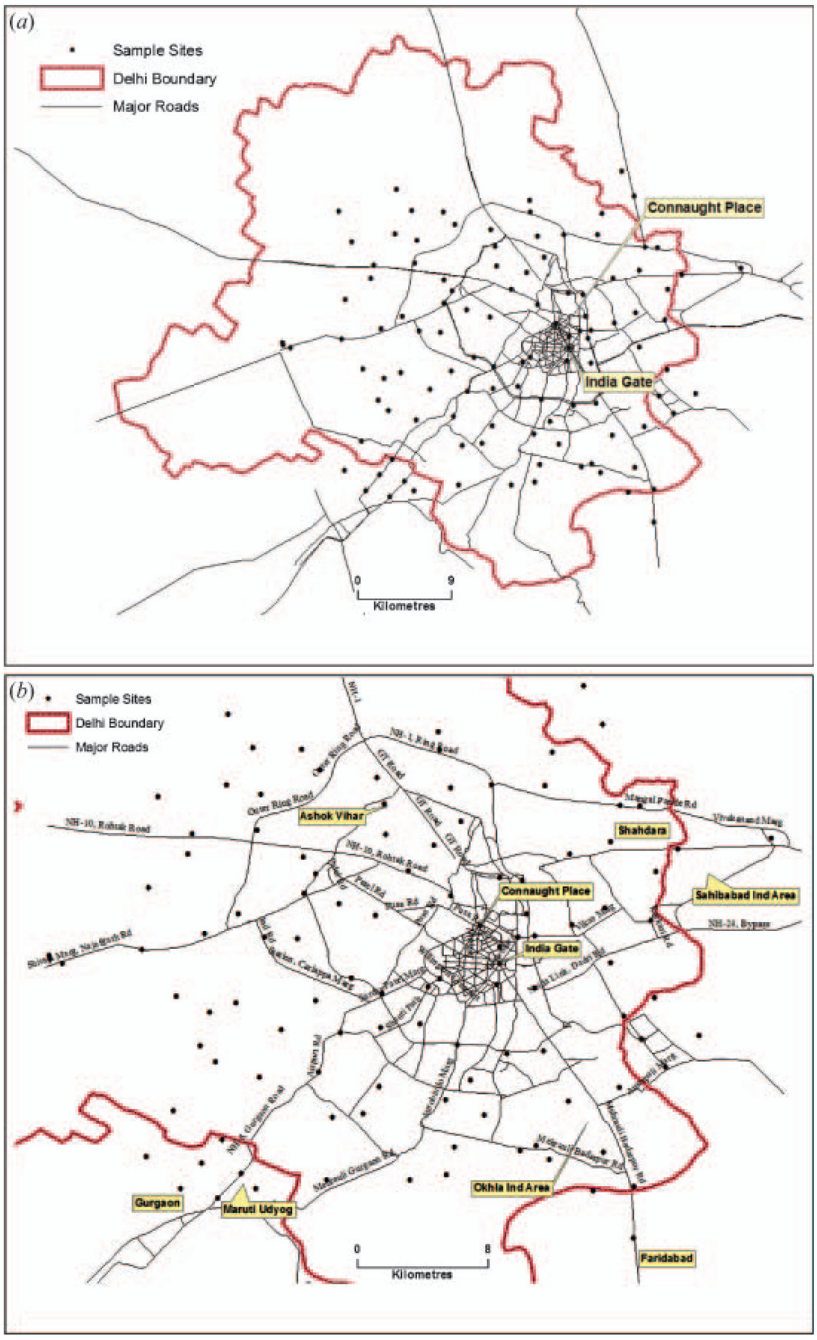

Figure 2.

Figure 2(*a*). The 113 air pollution monitoring sites in Delhi and its surroundings, July to December 2003. Figure 2(*b*). The 113 sample sites, key places and major roads in Delhi and its surroundings, July to December 2003.

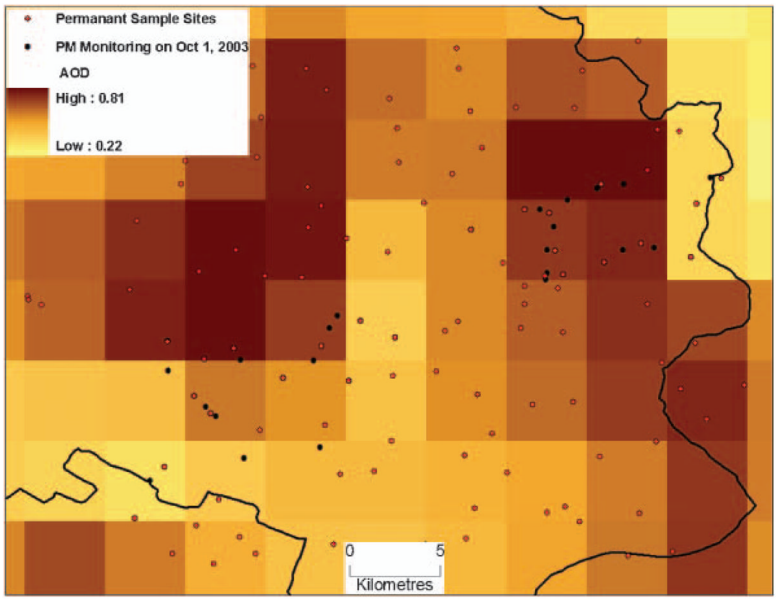

Figure 3.
Collocating 5 km AOD and point level PM data: AOD and PM estimates on 1 October 2003. AOD (τ_a) = $l_n(I_o/I)$ where l_o = intensity of radiation from the earth surface, l_s = intensity of radiation reaching the sensor, τ_a = optical depth in the presence of aerosols.

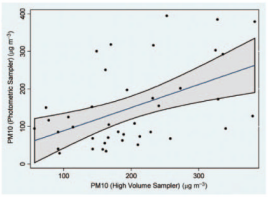

Figure 4.
PM_{10} from photometric and gravimetric samplers at ITO, Delhi, 23 July to December 2003.

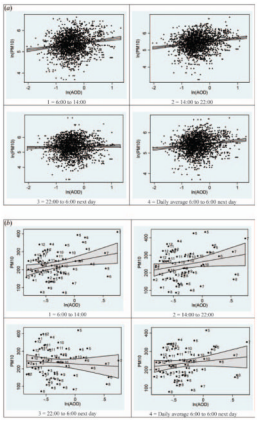

Figure 5.
(*a*). PM_{10} and AOD data at the ITO, Delhi, 2000 to 2005. Figure 5(*b*). Monthly PM_{10} and AOD data at the ITO, Delhi, 2000 to 2005. Number on the plot represents month of the year (1=January … 12=December).

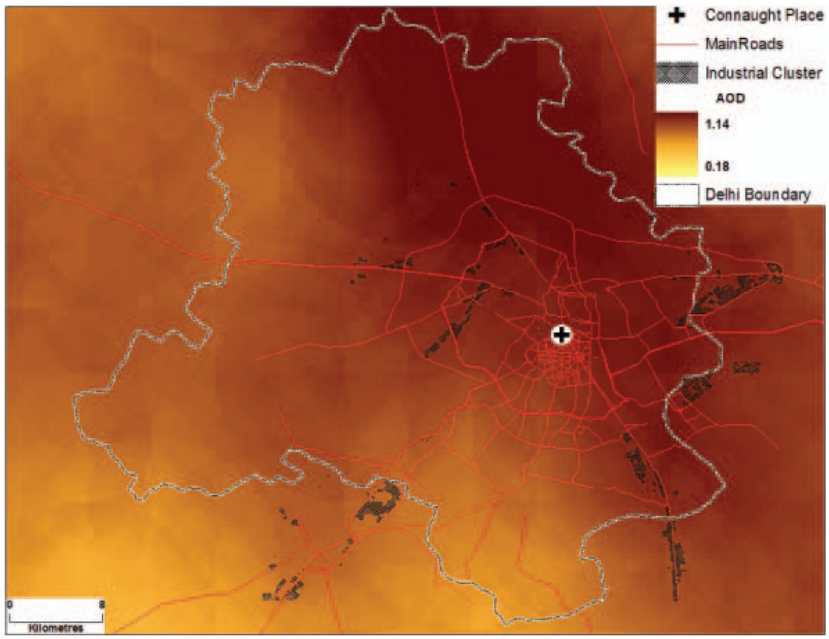

Figure 6.
AOD distribution in Delhi and surroundings, September to November 2003 (5 km spatial resolution).

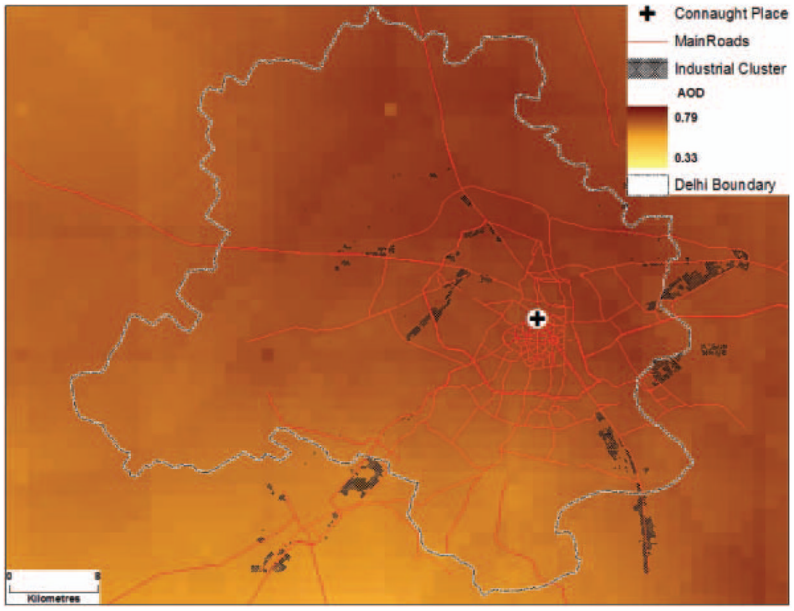

Figure 7.
AOD distribution in Delhi and surroundings, September to November 2003 (10 km spatial resolution).

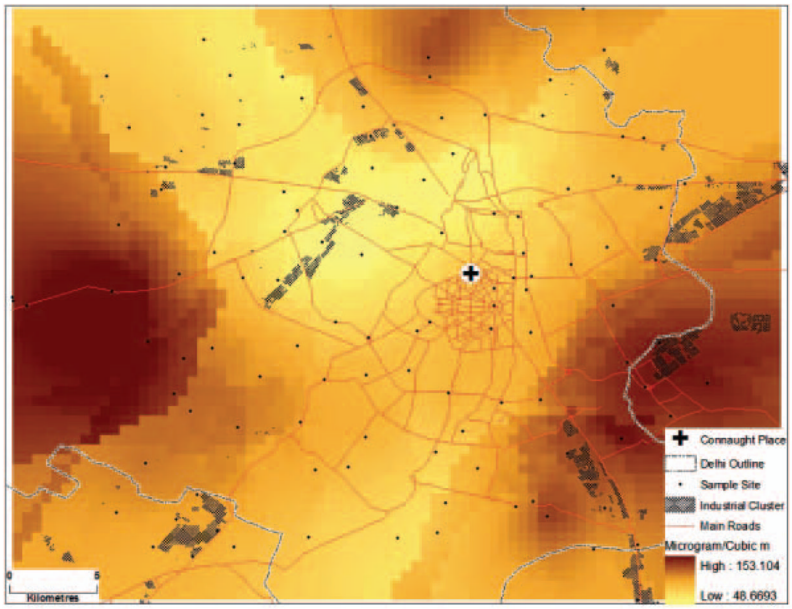

Figure 8.
$PM_{2.5}$ ($\mu g\ m^{-3}$) distribution in Delhi and its environs, July to November 2003.

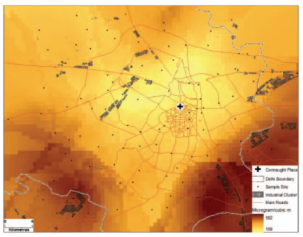

Figure 9.
PM_{10} (μg m^{-3}) distribution in Delhi and its environs, July to November 2003.

Table 1

Descriptive statistics of $PM_{2.5}$, PM_{10} and AOD data at 5 and 10 km spatial resolutions from August to November 2003.

	$PM_{2.5}$ ($\mu g\ m^{-3}$)		PM_{10} ($\mu g\ m^{-3}$)		AOD (5 km)*		AOD (10 km)	
Statistical parameter	**Delhi**	**Outside Delhi**	**Delhi**	**Outside Delhi**	**Delhi**	**Outside Delhi**	**Delhi**	**Outside Delhi**
Minimum	30.5	70.0	117.7	172.1	0.548	0.549	0.611	0.603
Mean	82.9	95.7	304.2	466.5	0.647	0.612	0.662	0.636
Maximum	268.4	167.8	850.3	957.9	0.714	0.685	0.693	0.680
Standard deviation	38.8	26.9	148.4	229.7	0.038	0.051	0.019	0.031
Skewness	1.8	1.5	1.3	0.6	−0.509	0.334	−0.613	0.369
Kurtosis	7.7	5.0	4.5	2.6	2.415	1.511	2.636	1.343
Coefficient of variation	46.9	28.1	48.8	49.2	5.9	8.3	2.9	4.8

Table 2

Distance from the city centre and the distribution of AOD and PM data, August to November 2003 (*n*=number of observations).

	AOD				PM (μg m^{-3})		
	AOD (5 km spatial resolution)		AOD (10 km spatial resolution)				
Distance from the city centre (°)	*n*	Mean	*n*	Mean	No. of sites	$PM_{2.5}$	PM_{10}
0.1	13	0.664 ± 0.040	3	0.687 ± 0.169	47	75 ± 8	263 ± 40
0.2	39	0.649 ± 0.028	10	0.673 ± 0.048	59	99 ± 17	391 ± 62
0.3	63	0.600 ± 0.020	16	0.634 ± 0.029	7	103 ± 38	380 ± 144
0.4	89	0.576 ± 0.018	22	0.633 ± 0.025		NA	NA
0.5	127	0.545 ± 0.013	62	0.623 ± 0.012		NA	NA
Inside Delhi	55	0.640 ± 0.023	23	0.657 ± 0.025	98	82.9 ± 7.8	304.2 ± 29.8

Table 3(a)

Regression of $PM_{2.5}$ on AOD, mean sea level pressure and relative humidity at 5 km pixel resolution – disaggregate analysis.

	Interval across satellite crossing time (h: min)										
$PM_{2.5}$ as a function of:	**0:15**	**0:30**	**0:45**	**1:00**	**1:15**	**1:30**	**1:45**	**2:00**	**2:15**	**2:30**	**All**
ln(AOD)	0.43 (2.77)**	0.449 (3.70)**	0.521 (5.05)**	0.491 (5.35)**	0.497 (5.62)**	0.451 (5.61)**	0.427 (5.41)**	0.419 (5.56)**	0.401 (5.33)**	0.398 (5.17)**	0.398 (5.18)**
Relative humidity (%)	0.024 (1.97)*	0.014 (−1.72)	0.012 (−1.87)	0.011 (−1.85)	0.018 (3.31)**	0.019 (4.51)**	0.019 (4.92)**	0.02 (5.48)**	0.021 (6.05)**	0.023 (6.59)**	0.024 (6.65)**
Mean sea level atmospheric pressure (hectopascal)	0.075 (3.37)**	0.072 (4.42)**	0.07 (5.09)**	0.063 (5.07)**	0.066 (5.71)**	0.067 (6.12)**	0.065 (6.13)**	0.067 (6.74)**	0.066 (6.68)**	0.07 (6.84)**	0.07 (6.85)**
Constant	−72.9 (3.21)**	−69.5(4.18)**	−66.8 (4.80)**	−59.6 (4.75)**	−63.7 (5.39)**	−64.1 (5.79)**	−62.4 (5.79)**	−64.4 (6.39)**	−63.8 (6.34)**	−67.2 (6.51)**	−67.2 (6.52)**
Observations	129	231	347	423	515	589	652	708	745	760	762
Number of AOD pixels	74	104	141	164	191	210	226	237	246	248	248
Pixel R^2	0.76	0.76	0.71	0.74	0.73	0.72	0.72	0.74	0.75	0.70	0.70

Table 3(b)

Regression of PM_{10} on AOD, mean sea level pressure and relative humidity at 5 km pixel resolution – disaggregate analysis.

	Interval across satellite crossing time (h: min)										
PM_{10} as a function of:	**0:15**	**0:30**	**0:45**	**1:00**	**1:15**	**1:30**	**1:45**	**2:00**	**2:15**	**2:30**	**All**
ln(AOD)	0.124 (−0.77)	0.159 (−1.18)	0.252 (2.26)*	0.254 (2.52)*	0.326 (3.43)**	0.29 (3.37)**	0.25 (3.06)**	0.227 (2.86)**	0.213 (2.65)**	0.207 (2.58)**	0.208 (2.59)**
Relative humidity (%)	0.017 (−1.31)	0.011 (−1.11)	0.005 (−0.66)	0.001 (−0.19)	0.004 (−0.61)	0.006 (−1.33)	0.006 (−1.42)	0.006 (−1.57)	0.008 (−1.95)	0.01 (2.46)*	0.01 (2.53)*
Mean sea level atmospheric pressure (hectopascal)	0.031 (−1.36)	0.033 (−1.78)	0.043 (2.88)**	0.038 (2.83)**	0.035 (2.83)**	0.038 (3.25)**	0.033 (3.06)**	0.036 (3.46)**	0.038 (3.59)**	0.042 (3.91)**	0.042 (3.92)**
Constant	−26.8 (−1.15)	−27.8 (−1.5)	−37.9 (2.51)*	−33.3 (2.42)*	−30.5 (2.40)*	−33.0 (2.80)**	−28.6 (2.58)**	−31.4 (2.96)**	−33.3 (3.10)**	−36.9 (3.43)**	−36.9 (3.44)**
Observations	129	231	347	423	515	589	652	708	745	760	762
Number of AOD pixels	74	104	141	164	191	210	226	237	246	248	248
Pixel R^2	0.85	0.80	0.63	0.64	0.68	0.63	0.69	0.69	0.66	0.66	0.64

Table 4(a)

Regression of $PM_{2.5}$ on AOD, mean sea level pressure and relative humidity at 5 km pixel resolution – aggregate analysis.

	Interval across satellite crossing time (h: min)										
$PM_{2.5}$ as a function of:	**0:15**	**0:30**	**0:45**	**1:00**	**1:15**	**1:30**	**1:45**	**2:00**	**2:15**	**2:30**	**All**
ln(AOD)	0.458 (3.23)**	0.482 (3.66)**	0.454 (4.24)**	0.369 (4.29)**	0.366 (4.46)**	0.371 (4.85)**	0.336 (4.77)**	0.333 (4.61)**	0.342 (4.93)**	0.352 (4.98)**	0.352 (4.99)**
Relative humidity (%)	0.037 (3.62)**	0.012 (−1.16)	0.01 (−1.32)	0.012 (−1.86)	0.013 (2.09)*	0.015 (2.72)**	0.017 (3.37)**	0.019 (3.98)**	0.016 (3.80)**	0.016 (3.66)**	0.016 (3.66)**
Mean sea level atmospheric pressure (hectopascal)	0.029 (−1.57)	0.054 (3.21)**	0.054 (4.06)**	0.052 (4.67)**	0.051 (4.86)**	0.051 (5.30)**	0.046 (4.92)**	0.047 (5.17)**	0.046 (5.11)**	0.047 (5.10)**	0.047 (5.10)**
Intra-pixel $PM_{2.5}$ variance	0.205 (10.77)**	0.178 (8.30)**	0.158 (9.40)**	0.144 (9.99)**	0.166 (11.27)**	0.173 (12.12)**	0.167 (12.36)**	0.159 (12.53)**	0.156 (12.65)**	0.162 (13.17)**	0.162 (13.15)**
Constant	−27.198 (−1.46)	−51.383 (3.02)**	−51.683 (3.82)**	−49.588 (4.39)**	−48.25 (4.58)**	−48.432 (5.01)**	−43.471 (4.63)**	−44.843 (4.88)**	−43.664 (4.80)**	−44.513 (4.80)**	−44.525 (4.80)**
Observations	37	58	94	109	126	142	155	167	174	175	175
R^2	0.81	0.66	0.61	0.61	0.62	0.63	0.62	0.61	0.6	0.61	0.61

Table 4(b)

Regression of $PM_{2.5}$ on AOD, mean sea level pressure and relative humidity at 5 km pixel resolution – aggregate analysis.

	Interval across satellite crossing time (h: min)										
PM_{10} as a function of:	**0:15**	**0:30**	**0:45**	**1:00**	**1:15**	**1:30**	**1:45**	**2:00**	**2:15**	**2:30**	**All**
ln(AOD)	0.179 (−1.00)	0.225 (−1.67)	0.28 (2.83)**	0.297 (3.53)**	0.271 (3.56)**	0.248 (3.35)**	0.204 (3.02)**	0.188 (2.81)**	0.165 (2.57)*	0.165 (2.56)*	0.166 (2.58)*
Relative humidity (%)	0.016 (−1.22)	0.009 (−0.9)	−0.004 (−0.58)	−0.004 (−0.64)	−0.003 (−0.5)	0 (−0.03)	0.003 (−0.63)	0.002 (−0.48)	0.003 (−0.76)	0.003 (−0.76)	0.003 (−0.77)
Mean sea level atmospheric pressure (hectopascal)	0.024 (−1.06)	0.035 (2.10)*	0.032 (2.62)*	0.031 (2.82)**	0.026 (2.66)**	0.026 (2.83)**	0.019 (2.09)*	0.019 (2.30)*	0.019 (2.35)*	0.02 (2.46)*	0.02 (2.46)*
Intra-pixel PM_{10} variance	0.226 (6.66)**	0.195 (7.95)**	0.21 (11.32)**	0.194 (11.50)**	0.213 (14.30)**	0.196 (13.78)**	0.181 (14.02)**	0.19 (14.90)**	0.186 (15.09)**	0.187 (15.42)**	0.187 (15.42)**
Constant	−21.272 (−0.93)	−32.065 (−1.9)	−28.825 (2.31)*	−27.664 (2.45)*	−22.626 (2.27)*	−22.809 (2.42)*	−14.998 (−1.66)	−15.804 (−1.86)	−15.966 (−1.9)	−16.966 (2.02)*	−16.968 (2.02)*
Observations	37	59	94	110	127	142	155	167	174	175	175
R^2	0.59	0.59	0.62	0.58	0.66	0.61	0.6	0.6	0.6	0.61	0.61

Table 5

AOD within 0.1° radius of ITO and other pollutants (monitored by CPCB) at ITO in the pre- and post-regulation periods.

	Time/shift	2000–2002 (pre- and regulation implementation period)	2003–2005 (post-regulation period)	2000–2002 to 2003–2005 (pre- and post-regulation difference)
AOD (τ)	10:30 ± 0:30	0.80 (± 0.02)	0.71 (± 0.02)	−0.091 (± 0.060)
SO_2 $\mu g\ m^{-3}$ (95% CI)	6:00–14:00	13.4 (± 0.3)	9.1 (± 0.2)	−4.3 (± 0.8)
	14:00–22:00	17.5 (± 0.5)	10.3 (± 0.3)	−7.2 (± 1.1)
	22:00–6:00 (next day)	12.7 (± 0.4)	8.3 (± 0.2)	−4.4 (± 0.9)
NO_2 $\mu g\ m^{-3}$ (95% CI)	6:00–14:00	63.6 (± 1.1)	89.0 (± 1.4)	25.4 (± 3.5)
	14:00–22:00	81.0 (± 1.4)	104.1 (± 1.7)	23.1 (± 4.3)
	22:00–6:00 (next day)	63.2 (± 1.2)	88.4 (± 1.7)	25.2 (± 4.0)
PM_{10} $\mu g\ m^{-3}$ (95% CI)	6:00–14:00	218.7 (± 5.9)	248.1 (± 6.5)	29.4 (± 17.5)
	14:00–22:00	248.0 (± 6.9)	262.1 (± 7.1)	14.1 (± 19.8)
	22:00–6:00 (next day)	238.1 (± 7.9)	256.7 (± 7.8)	18.6 (± 22.5)
	24 h average	234.7 (± 5.8)	256.2 (± 6.1)	21.4 (± 16.8)
TSP	6:00–14:00	534.7 (± 12.7)	526.2 (± 11.2)	−8.5 (± 34.3)
$\mu g\ m^{-}{}_3$ (95% CI)	14:00–22:00	607.0 (± 13.9)	556.9 (± 11.7)	−50.2 (± 36.9)
	22:00–6:00 (next day)	523.8 (± 13.9)	508.8 (± 13.4)	−15.0 (± 38.8)
	24 h average	554.7 (± 11.3)	528.9 (± 9.9)	−25.8 (± 30.4)

Table 6

Monthly PM_{10} and TSP data as a function of monthly AOD data, 2000 to 2005.

	PM				TSP			
Covariates	**6:00–14:00**	**14:00–22:00**	**22:00–6:00**	**Daily (24 h mean)**	**6:00–14:00**	**14:00–22:00**	**22:00–6:00**	**Daily (24 h mean)**
ln(AOD)	185.51 (6.68)**	193.74 (5.65)**	151.09 (4.69)**	177.4 (6.25)**	287.01 (5.81)**	363.5 (6.19)**	258.25 (4.32)**	300.01 (5.96)**
Relative humidity (%)	−2.82 (4.92)**	−2.909 (4.11)**	−3.145 (4.73)**	−2.948 (5.03)**	−4.711 (4.62)**	−2.896 (2.39)*	−5.331 (4.32)**	−4.12 (3.97)**
Mean sea level atmospheric pressure (hectopascal)	8.337 (5.94)**	9.169 (5.29)**	11.401 (7.00)**	9.674 (6.74)**	9.168 (3.67)**	14.201 (4.79)**	13.369 (4.43)**	12.179 (4.79)**
Constant	−8011 (5.70)**	−8825 (5.09)**	−11 087 (6.80)**	−9346 (6.51)**	−8464 (3.39)**	−13 512 (4.55)**	−12 701 (4.20)**	−11 500 (4.52)**
Observations	66	66	66	66	66	66	66	66
R^2	0.52	0.44	0.52	0.53	0.48	0.41	0.38	0.45